SCIENTIFIC JOURNAL
OF MARITIME RESEARCH
[POMORSTVO]

University of Rijeka
FACULTY OF MARITIME STUDIES

https://doi.org/10.31217/p.39.2.9

Effect of Excessive Towing Load on The Motion and Tension Behaviour of 50,000 DWT Single Point Mooring System

Tuswan Tuswan[1*], Adam Adam[1], Alfiy Alfatarizqi[2], Ahmad Fauzan Zakki[1], Berlian Arswendo Adietya[1], Zulfaidah Ariany[3], Aulia Windyandari[3]

[1] Departemen Teknik Perkapalan, Fakultas Teknik, Universitas Diponegoro, Semarang, 50275, Indonesia, e-mail: tuswan@lecturer.undip.ac.id; adam.alfariza1@gmail.com; ahmadfauzanzakki@lecturer.undip.ac.id; berlianarswendoadiet@lecturer.undip.ac.id

[2] Departemen Sistem Perkapalan, Institut Teknologi Sepuluh Nopember, Surabaya, 60111, Indonesia, e-mail: alfiyalfatarizqi.research@gmail.com

[3] Departemen Teknologi Industri, Sekolah Vokasi, Universitas Diponegoro, Semarang, 50275, Indonesia, e-mail: zariany@live.undip.ac.id; auliawindyandari@lecturer.undip.ac.id

[*] Corresponding author

ARTICLE INFO

Original scientific paper
Received 24 April 2025
Accepted 2 June 2025

Key words:
Mooring analysis
Tension analysis
Single point mooring
Tanker

ABSTRACT

Catenary Anchor Leg Mooring (CALM) systems are vital for offshore oil and gas operations to moor Tankers and transfer cargo. A common issue arises when Tankers exceed the mooring system's design capacity, leading to shifts in the Single Point Mooring (SPM) coordinate. This study examines the structural integrity of a 50,000 DWT CALM-type SPM system under excessive mooring loads, simulating conditions with Tankers of 55,000, 75,000, and 100,000 DWT. The analysis follows API RP 2SK, DNV OS E301, ABS standards and includes three stages: (1) Hydrodynamic analysis to obtain the Response Amplitude Operator (RAO); (2) 3D coupled dynamic time-domain simulation to determine mooring line tension; and (3) Von Mises stress analysis of the Y-connection. Results show that increasing tow loads elevate mooring line tension, with the highest force found in Chain 1C under beam sea with a 100,000 DWT Tanker. The maximum stress occurs at the Y-connection in hole C facing the seabed, failing to meet safety requirements. These findings highlight the critical need for adherence to design load limits to ensure safe and reliable mooring system performance.

1 Introduction

Offshore oil and gas drilling requires robust facilities to support exploration and operations. Tankers are crucial in transporting oil and gas products from offshore sites to onshore facilities [1]. The marine environment, however, is complex and dynamic, leading to significant challenges, particularly the risk of mooring system failures on floating platforms [2]. A common issue is the shifting coordinates of floating platforms like SPM systems, often due to mooring forces that exceed their capacity. A mooring system must withstand environmental loads, including wind, waves, and currents, yet increased tension in SPM lines frequently leads to line failure [3], [4]. Previous studies have examined mooring failures, such as a mooring line failure on a Mobile Offshore Drilling Unit (MODU) under extreme conditions [5], tendon breakage on a Tension-Leg Platform (TLP) during moderate storm conditions [6], [7], mooring rope failure in oscillating water column devices under severe wave conditions [8], [9], [10], and safety concerns in FPSOs [11]. Environmental loads can induce movement in ship structures during unloading, placing additional stress on mooring systems [12]. Dynamic loads, coupled with the resulting damping force, significantly impact buoy motion [13], while excessive tension from vessel movement and environmental loads can disrupt unloading operations [14].

Several types of SPM systems are used offshore, including Catenary Anchor Leg Mooring (CALM) buoy, Single Anchor Leg Mooring (SALM), and Fixed Tower Articulated Loading Platform (ALP) [15]. The CALM buoy has demonstrated high efficiency in various offshore applications [16], [17], [18]. Its technical effectiveness is ev-

ident in loading and offloading processes at terminals worldwide and in mooring system tools supporting cargo extraction [19]. The CALM buoy system's technology and economic viability have also advanced, making it a preferred choice for many offshore operators. SPM systems are versatile, suitable for different water depths, and adaptable to marine environments [20]. Large vessels, such as Very Large Crude Carriers (VLCCs), can moor to SPMs using a mooring hawser [21]. However, dynamic analysis of the SPM CALM buoy remains complex due to environmental loads and the intricate interactions between the buoy, hawser, moored Tanker, mooring line, and riser [22], [23].

The SPM structure operates as an integrated floating system for cargo transfer by connecting a floating hose to the Tanker manifold, which channels the flow to the Pipe End Manifold (PLEM) [24]. Generally, SPM components include mooring lines, connectors, and anchors integrated with the mooring system. These mooring lines consist of various elements, such as chains, fiber ropes, and standard ropes [25]. CALM systems, introduced in 1985, now serve approximately 85% of the world's 700 oil terminals, with significant operations in Southeast Asia, the Middle East, and West Africa [26], [27]. CALM buoys are widely used to load efficiently spread-moored Floating Production Storage and Offloading (FPSO) vessels due to their robust flow capabilities, assisting FPSOs in transferring oil to shuttle Tankers [28]. In essence, the SPM CALM buoy functions as both a ship mooring system and a terminal for distributing offshore-extracted oil, integrated with the PLEM [29]. Several previous investigations have been reviewed. Qi et al. [30] conducted related research on stress measurement, focusing on the skirt geometry of the CALM buoy and subsea hose system. They analyzed three models to study skirt dimensions, using a "Chinese lantern" configuration for the riser, and employed Ansys AQWA software. The results indicated that the skirt dimensions significantly impact hydrodynamic properties, such as heave motion, affecting the buoy's performance in heave control.

This study investigates the structural performance of a 50,000 DWT CALM-type Single Point Mooring (SPM) system subjected to excessive mooring loads by simulating scenarios involving Tankers of 55,000, 75,000, and 100,000 DWT. The assessment is conducted in accordance with API RP 2SK, DNV OS E301, and ABS standards, and comprises three main phases: (1) hydrodynamic analysis to derive the Response Amplitude Operator (RAO); (2) 3D coupled dynamic time-domain simulation to evaluate mooring line tensions; and (3) von Mises stress analysis focused on the Y-connection. This study is limited to analyzing the structural integrity of the Y-connection within a 50,000 DWT CALM system under increased loading from larger Tankers. Although the analysis considers mooring tensions and stress responses in compliance with established standards, it does not address factors such as long-term fatigue behavior, soil-structure interaction, or variations in environmental loading conditions.

2 Models and Methods

2.1 Reference Model & Specification

The data supporting this research includes buoy, Tanker, mooring line, Y-connection/ shackle, and environmental data. The main subject is the SPM CALM buoy Arubay, owned by Pertamina Lte, with a 50,000 DWT capacity in the North Sumatra Sea, Indonesia. Table 1 and Figure 1 provide the main dimensions and detailed models.

Table 1 Principal dimension data of SPM CALM buoy Arubay.

Parameters	Value	Unit
Holding capacity	50,000	ton
Displacement (Δ)	491.782	ton
Inside diameter (DI)	11.38	m
Outside diameter (DII)	14.78	m
Height (H)	4.55	m
Draft (T)	2.835	m
Centre of gravity (CoG) in Z-axis	2.33	m
X-mass radius of gyration	3.101	m
Y-mass radius of gyration	3.101	m
Z-mass radius of gyration	3.982	m

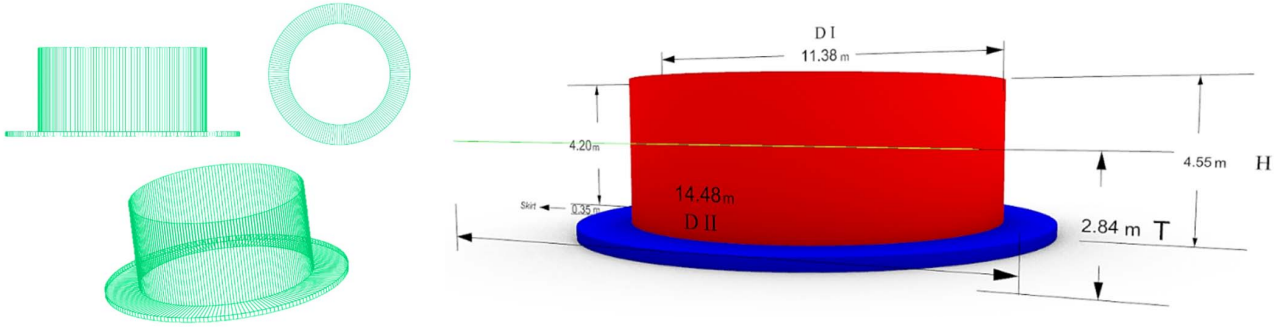

Figure 1 3D geometry model of SPM CALM buoy Arubay.

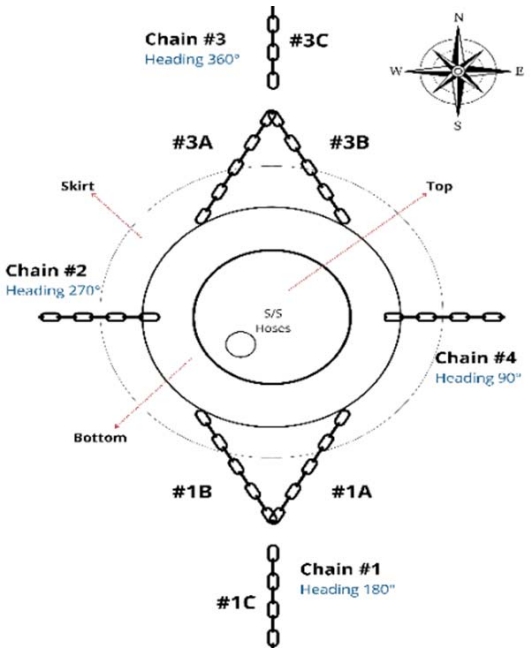

(a)

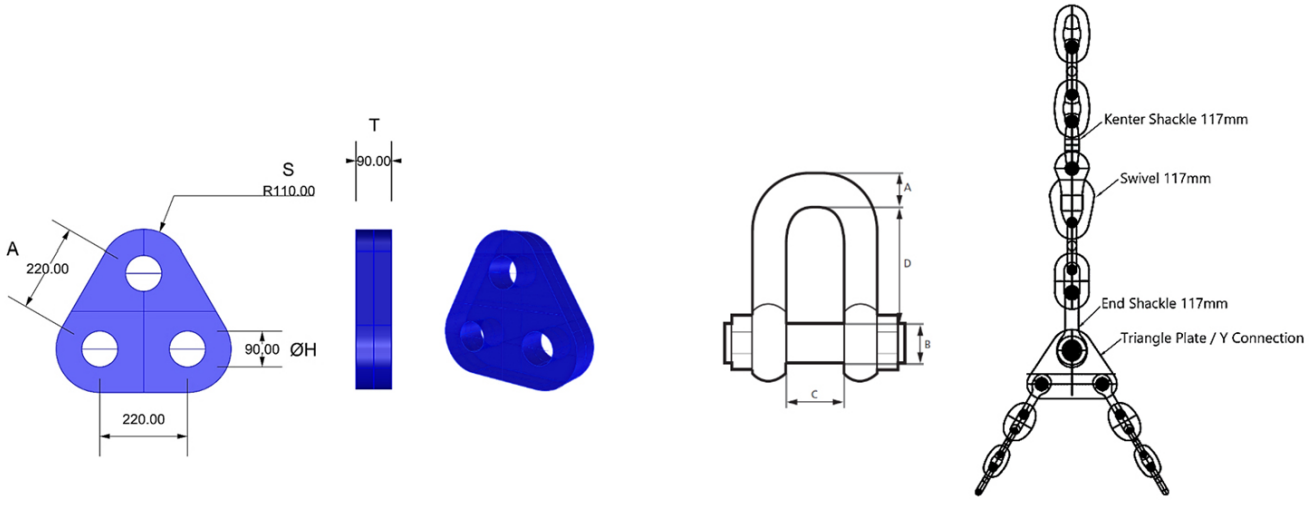

(b)

Figure 2 (a) Mooring line system, (b) Y-connection plate and shackle

Table 2 Mooring line data of SPM CALM buoy

Chain components	Riding stud link chain Grade 2	
	Chain length (m)	Chain diameter (mm)
Chain 1A	22.498	76
Chain 1B	21.906	76
Chain 1C	220.068	76
Chain 2	169.731	78
Chain 3A	22.075	73
Chain 3B	21.820	76
Chain 3C	117.951	76
Chain 4	122.755	75

In the SPM CALM buoy system, the mooring line and Y-connection plate are crucial for maintaining stability and load distribution [31]. The mooring line, often a steel chain or wire rope, anchors the buoy and withstands dynamic marine forces. The Y-connection plate joins two mooring lines and distributes loads efficiently, minimizing stress points and reducing fatigue risk. The Y-connection connects this plate to the lines, allowing pivot movement to adjust to sea conditions. Each component is carefully specified in Tables 2 and 3 to ensure durability and reliable performance under varying marine loads.

Table 3 Specifications of Y-connection plate and shackle

Y-connection plate parameter		
Parameters	**Value**	**Unit**
A	220	mm
ØH	90	mm
T	90	mm
S	110	mm
Minimum breaking load (MBL)	425	tons
Shackle parameters		
A	75	mm
B	82	mm
C	127	mm
D	230	mm
Shackle weight (W)	60	kg
Safety working load (SWL)	85	tons

SPM is a stationary offshore mooring and loading system that securely allows Tankers to anchor at a single point in the open sea. In real operation in the North Sumatra Sea, Indonesia, the SPM CALM buoy Arubay owned by Pertamina Lte is operated with an excessive loading capacity above 50,000 DWT Tanker, so performance evaluation is critical to ensure safe operation. In this case, three Tankers with different DWT, namely 55,000 DWT (MT. Califura), 75,000 DWT (MT. Athens Star), and 100,000 DWT (MT. Gunung Geulis), are compared in Table 4.

Table 4 Principal dimension data of Tankers

Parameters	**Model 1**	**Model 2**	**Model 3**
Ship name	MT. Califura	MT. Athens Star	MT. Gunung Geulis
Deadweight tonnage (DWT), ton	55000	75000	100000
Length overall (LOA), m	183	228.6	237.76
Breadth (B), m	32.2	32.26	42
Height (H), m	19.1	20.8	21.3
Draft (T), m	11	14.45	12.19

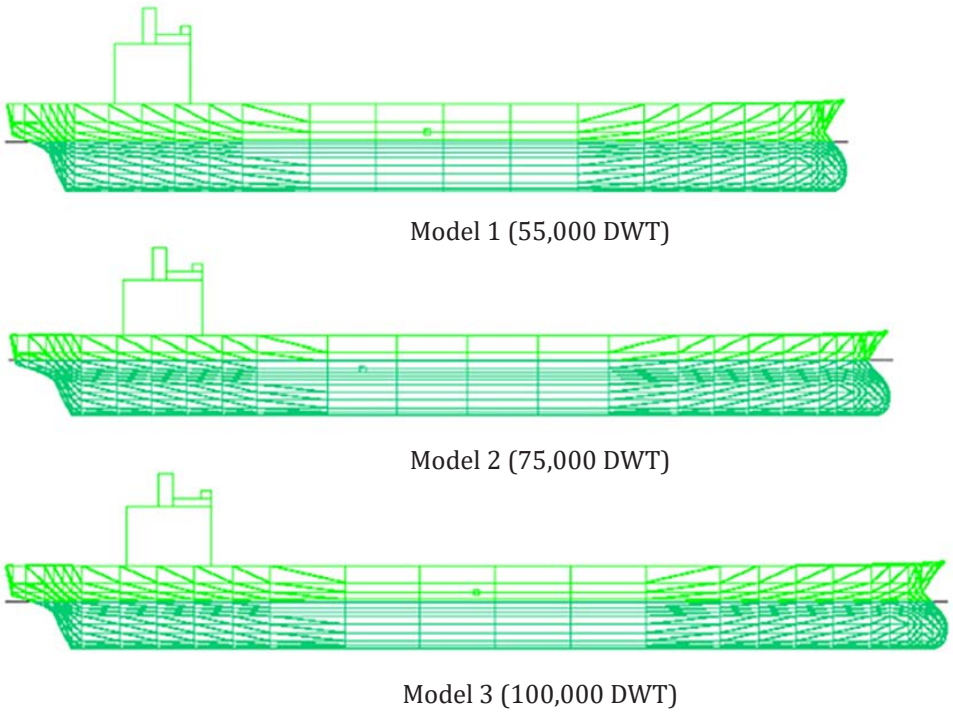

Figure 3 Geometry model of three Tankers with different DWTs

2.2 3D Time Domain Analysis

This research utilizes MOSES 8.0 and OrcaFlex 9.2 to model and analyze tension in each mooring line and the Y-connection plate. MOSES is commonly used for hydrostatic and hydrodynamic analysis of offshore platforms and vessels, enabling efficient simulations for transportation, installation, and in-place design of floating systems. Its integrated solver streamlines analysis and minimizes errors compared to multi-software workflows. Furthermore, OrcaFlex is widely used for the dynamic analysis of offshore marine systems, providing accurate simulations of catenary systems such as flexible risers and umbilical cables under currents, wave loads, and motion. It offers extensive graphic outputs, batch mode for routine analyses, and fatigue analysis post-processing capabilities.

Related 3D time domain analysis allows non-linearity for all conditions in the motion equation. High and low-frequency excitation waves are applied simultaneously in the time domain. In simplified form, the equations of motion for a mooring system with six degrees of freedom can be expressed by Equations 1 and 2.

$$\sum_{j=1}^{6}\{(M_{ij}+a_{ij}).\ddot{x}+b.\dot{x}+c.x\}=F_i \tag{1}$$

$$F = F_m + F_w + F_l \tag{2}$$

where x is the displacement matrix, M is a mass matrix, a is the added mass matrix, c is the hydrostatic stiffness matrix, exists only for heave roll and pitch components, F is the force matrix including wind, current, first & second order wave forces, F_m is a steady (mean) component of force, F_w is wave frequency component of force, F_l is a low-frequency component of force.

In some mooring analyses, the mooring system's dynamic loads, wave frequency, and low-frequency ship motion are directly combined. Hence, the mooring system not only applies the restoring force but can also apply damping and inertial-type loads to the ship.

2.3 Response Amplitude Operator (RAO)

Response Amplitude Operator (RAO) output provides critical information on ship motion characteristics and SPM behavior. Typically, RAO data is presented as a comparison result showing the relationship between RAO translation and its period, as represented in Equation 3 [32].

$$RAO(\omega) = \frac{\zeta k0(\omega)}{\zeta 0(\omega)} \tag{3}$$

RAO equation varies between translational motion (surge, heave, sway) and rotational motion (yaw, roll, pitch). For translational motion, RAO is defined as the ratio of the translational motion amplitude to the incident wave amplitude, calculated using Equation 4 [32].

$$RAO(\omega) = \frac{\zeta k0}{\zeta 0} \tag{4}$$

For rotational motion, the RAO formulation is the ratio of the rotational motion amplitude to the wave slope, which is calculated by multiplying the wave number with the incident wave, as shown in Equation 5 [32].

$$RAO(\omega) = \frac{\zeta k0}{\zeta 0} = \frac{\left(\frac{\omega^2}{g}\right)\zeta k0}{\zeta 0} \tag{5}$$

The environmental data used in this study consists of field measurements, including wind and wave data from North Sumatra, Indonesia, as shown in Table 5.

Table 5 Environmental data for annual operating conditions [33].

Environmental criteria	Condition value	
	(10 year condition)	(100 year condition)
Maximum wave height (Hmax)	2.939 m	3.102 m
Significant wave height (Hs)	1.58 m	1.668 m
Top period (Tp)	5 s	5 s
Wave velocity (v)	2 knots	2 knots

2.4 Procedure of Motion Simulation

The SPM mooring analysis was conducted in two stages. The first stage involved hydrostatic and hydrodynamic analyses using MOSES software to obtain the RAO response for both the ship and the SPM. The second stage focused on time-domain analysis with OrcaFlex, utilizing the ship motion responses from the first stage to determine the maximum tensions in the mooring line and Y-connection. In the first stage, the ship's motion response was derived from 3D diffraction theory analysis. The hull shape was modeled with a full-scale refined mesh, with panels representing the hull surface. Hydrostatic analysis was conducted to obtain buoy hydrostatic data. These results were validated against each ship's stability booklet to ensure model accuracy.

After validating the hydrostatic results from the hydrodynamic analysis, velocity potentials for each panel were generated based on the interaction with the sea, creating a pressure database. The first six velocity potentials arise from the unit motion of the vessel body at a given frequency for each degree of freedom. The remaining potentials are due to the ship's body disrupting the waves, referred to as diffraction potentials. These diffraction potentials depend on both the wave frequency and the direction of wave incidence. All potentials are

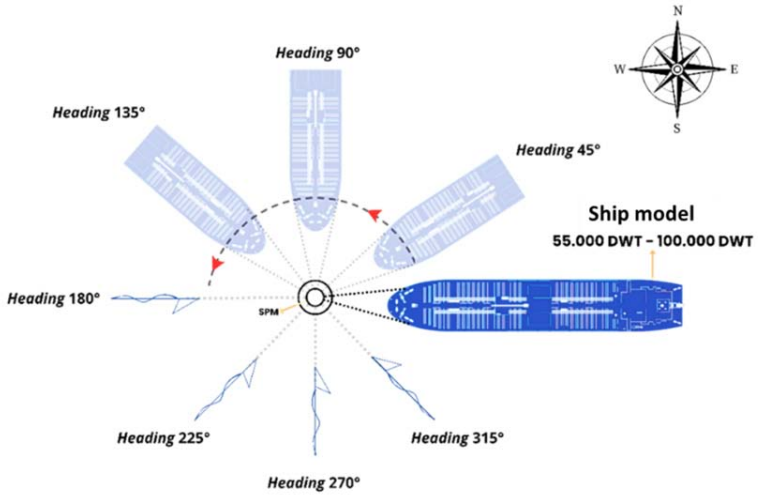

Figure 4 Simulation configuration between SPM and Tanker with different operating conditions.

represented as complex numbers, encompassing real and imaginary components. Finally, the required motion responses were calculated from the pressure database, including RAO, quadratic transfer function (QTF), added mass, and damping force.

The second phase involved a fully integrated 3D finite element and time-domain dynamic analysis of the mooring system. This model accounts for all contributions of the mooring line to the behavior and response of the entire system, including added mass, damping, stiffness, and low and high-frequency dynamic loads that vary with time, depth, and direction of incident external forces. The ship is modeled as a rigid body, with its motion derived from the responses obtained in the 3D diffraction theory analysis. The ship reacts to waves at two distinct frequencies: the first frequency corresponds to the wave frequency and results from wave loads, which are linear functions of wave amplitude. This first frequency motion is represented as the RAO.

The SPM CALM buoy is modeled by considering its shape, diameter, and height to achieve the appropriate displacement and buoyancy while providing damping for wave-induced motions. Damping forces and moments are applied to represent this effect [34]. To ensure that the physical and hydrodynamic properties of the CALM buoy are accurately represented, the modeling must closely resemble real-world conditions, incorporating parameters such as drag force, added mass, and the buoy's center of gravity. The modeling utilizes 3D buoy objects created with OrcaFlex software.

The mooring line is modeled explicitly using finite element techniques, considering the non-linear shape of their 3D catenaries due to environmental and external loads, as illustrated in Figure 4. Additionally, tension analysis is conducted using Inventor software to measure the maximum stress on the Y-connection, which will be discussed in Section 3.3.

2.5 Tension Analysis on SPM Mooring System

In the API RP 2SK 4th edition [35], mooring system strength is assessed under two load scenarios: the Ultimate Limit State (ULS) and the Accidental Limit State (ALS). The ULS evaluation ensures that mooring lines can withstand extreme environmental loads without failure [36]. This analysis applies the most severe conditions, with all mooring lines fully intact and operational. In contrast, ALS analysis verifies that the system can handle unexpected failures, simulating one mooring line being freely disconnected (known as a "one-line damaged" analysis) to confirm the remaining system's resilience under operational conditions.

This study assesses operability based on the mooring buoy's performance under 10-year environmental conditions, ensuring it meets the API RP 2SK safety factor of 1.67 for ULS conditions [35]. Additionally, SPM behavior is analyzed in survival mode (free-floating without a Tanker) under 100-year environmental loads, with wave directions matching operational conditions. The safety factor is determined by comparing the minimum breaking load to the maximum tension experienced by the mooring components [37].

2.6 Strength Assessment Criteria

Assessment criteria are standards used to evaluate performance, ability, or quality in the assessment process. These criteria offer clear guidance on knowledge, skills, and expected qualities. This study applied two assessment criteria, focusing on the minimum safety factor limits for the mooring line and Y-connection. Table 6 presents the safety criteria under both operating and survival conditions. The result provides assessment criteria for operating and survival conditions based on two key parameters: the minimum breaking load for a 76

Table 6 Assessment criteria for operating and survival conditions

Parameter criteria	Standard	Safety factor	Max. allowable
Minimum breaking load (76 mm diameter chain)	API RP 2SK and DNV OS E301 [35], [38]	1.67	284.093 T
Yield strength of Y-connection	ABS standard [39]	1	275.8 MPa

mm diameter chain and the yield strength of the Y-connection. This criterion indicates that the mooring line must withstand 1.67 times the maximum expected load under operating conditions, with a maximum load limit of 284.093 tons. Moreover, Y-connection is assessed to handle loads up to its yield strength without any additional safety factor, implying that it should not exceed 275.80 MPa under operating or survival conditions.

3 Results and Discussion

3.1 Model Parameter Validation

Validation was conducted to verify the accuracy of the DWT, weight, and displacement parameters for the SPM and Tankers. According to the ABS Rules for Building and Classing Mobile Offshore Drilling Units (MODU) 1998 [39], the displacement error should not exceed 2%, while other parameters should have an error within 1% [39]. The validation results confirm that the structural model is suitable for analyzing regular wave motion characteristics. This motion analysis was performed in the frequency domain for a free-floating structure without a mooring system. Detailed validation results are presented in Table 7. It can be found that there is a good agreement between the developed model and the exact value with an error below 1%.

3.2 Hydrodynamic Response of Tanker and SPM

Figure 5 presents a comparative analysis of pitch RAO responses for three Tankers with 55,000, 75,000, and 100,000 DWT. Each vessel's pitch RAO is measured across different wave headings. These RAO responses reflect how each vessel's pitch motion varies with wave frequency and heading, providing insight into the impact of vessel size on pitch dynamics. Across all headings, a consistent trend emerges where each vessel's pitch RAO peaks near a frequency of approximately 0.70 rad/s. This suggests that 0.70 rad/s is a resonant frequency for pitch motion, a point at which the vessels are most susceptible to pitch movement. As frequency increases beyond this peak, the RAO values for all DWTs diminish significantly, indicating a reduced response to higher-frequency waves.

When comparing the RAO amplitudes across different DWTs, a relationship between vessel size and pitch response is evident. The 55,000 DWT vessel consistently shows the highest pitch amplitude, especially in the frequency range between 0.5 and 0.75 rad/s, suggesting that smaller vessels are more responsive to wave-induced pitch motion. This heightened response can be attributed to the lower mass and smaller moment of inertia of the 55,000 DWT Tanker, making it more sensitive to wave forces. Conversely, the 100,000 DWT vessel exhibits the lowest amplitude across all headings, indicating that larger Tankers experience less pronounced pitch motion due to their greater mass and inertia, which contribute to dampening the pitch response.

The effect of wave heading on pitch motion is also notable. In stern seas (0°) and following seas (180°), the 55,000 and 75,000 DWT vessels show marked peaks near the resonant frequency of 0.75 rad/s, while the 100,000 DWT vessel's peak is more subdued. This disparity underscores that smaller vessels are more affected by waves coming from the fore or aft, while the larger vessel's pitch remains more stable under similar conditions. In contrast, when waves approach from beam seas (90°), all vessels demonstrate relatively low RAO amplitudes, indicating that pitch motion is minimal when waves strike broadside, likely due to the nature of pitch response being less influenced by lateral wave forces. In quartering seas, at 45° and 135°, the pitch responses for the 55,000 DWT vessel again exceed those of the larger Tankers, suggesting that quartering waves can provoke noticeable pitch motion in smaller vessels while larger vessels remain comparatively stable.

Table 7 Validation test result of model parameters

Object	Parameters	Exact value	Model	Unit	Error (%)
SPM	Weight	274.698	275.849	MT	0.01151
	Displacement	491.782	492	MT	0.00218
55,000 DWT Tanker	DWT	55.000	54.692	tons	0.00308
75,000 DWT Tanker		75.000	75.571	tons	0.00571
100,000 DWT Tanker		100.000	105.322	tons	0.05322

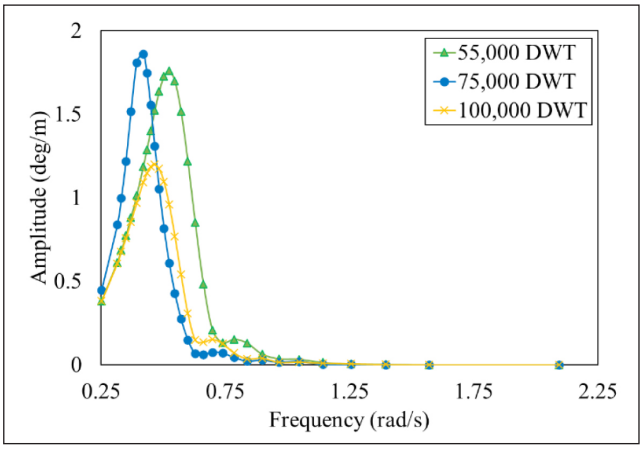

(a)

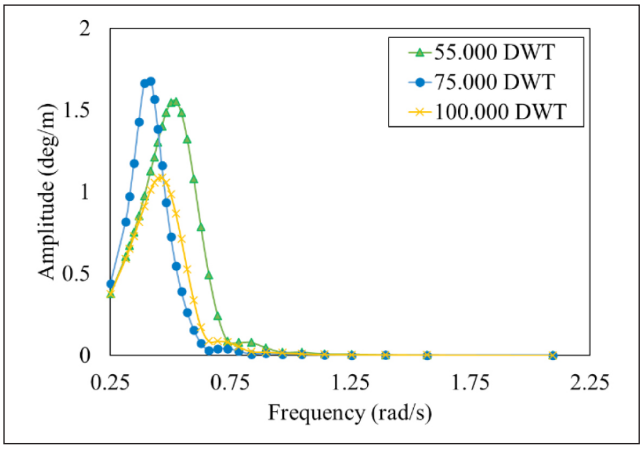

(b)

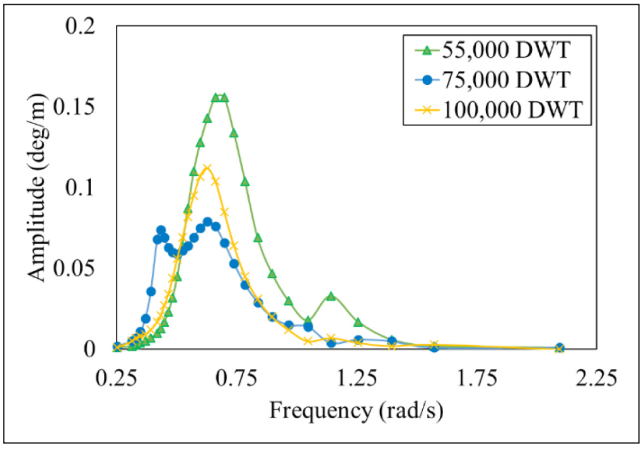

(c)

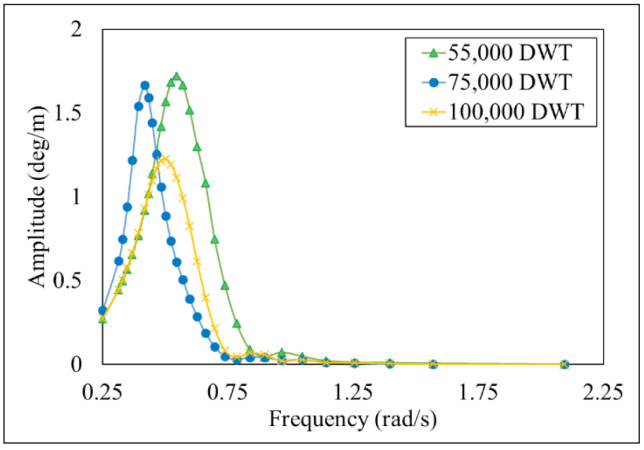

(d)

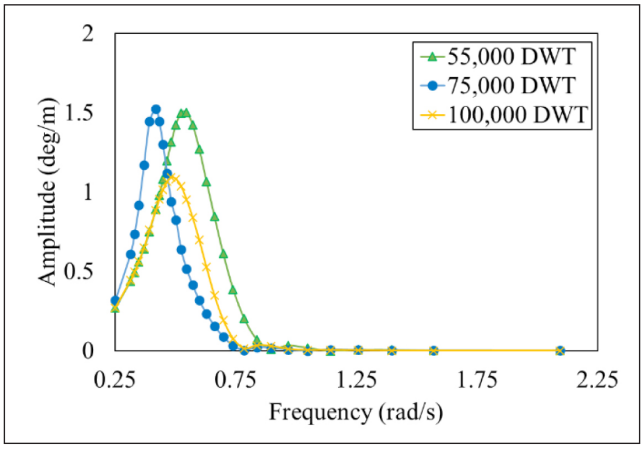

(e)

Figure 5 Comparison of pitch RAO motions, a) stern seas (0°), b) following sea (180°), c) beam sea (90°), d) quartering seas (45°), and e) quartering sea (135°).

Figure 6 illustrates the heave RAO responses for three Tankers with different deadweight tonnages. These heave RAO responses are analyzed across wave headings, with each subplot representing a different heading angle. These heave RAO graphs reveal that all three Tankers exhibit a peak in heave response at low frequencies, around 0.5 rad/s, with the amplitude gradually decreasing as frequency increases. The 55,000 DWT vessel shows slightly higher heave responses than the larger vessels, indicating greater susceptibility to

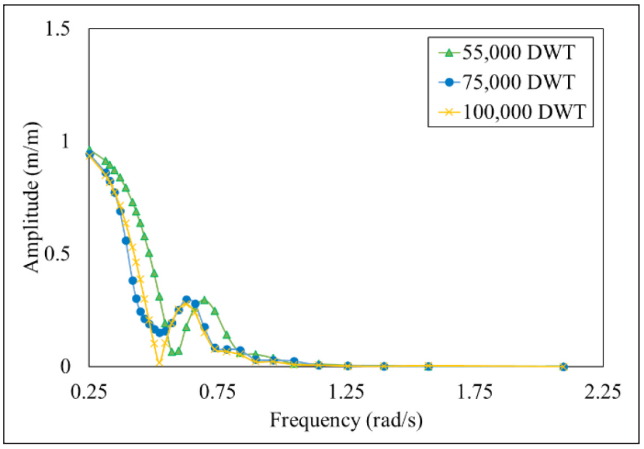

(a)

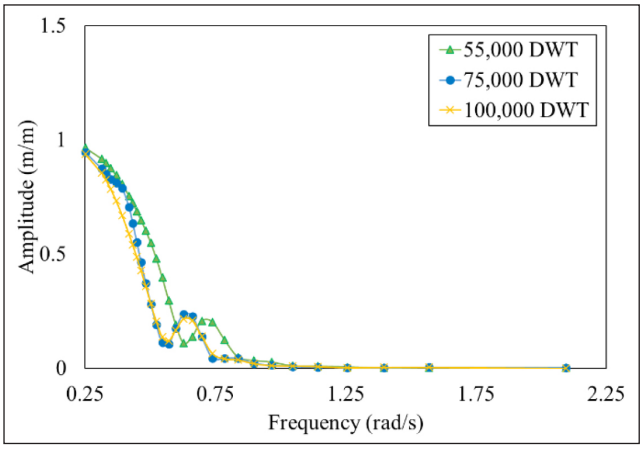

(b)

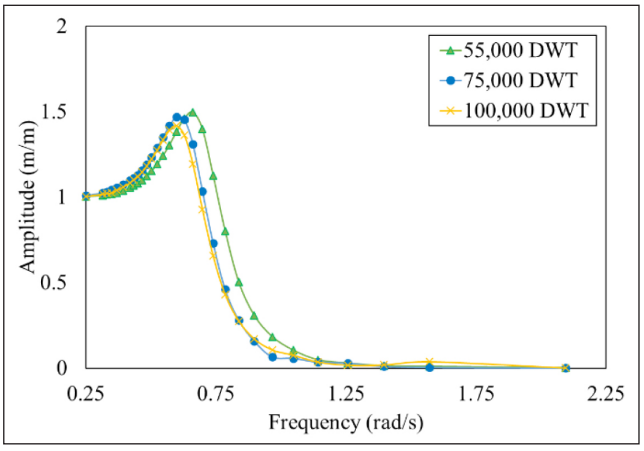

(c)

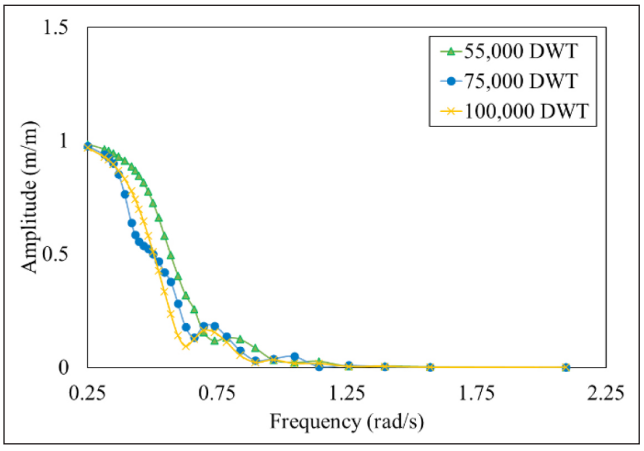

(d)

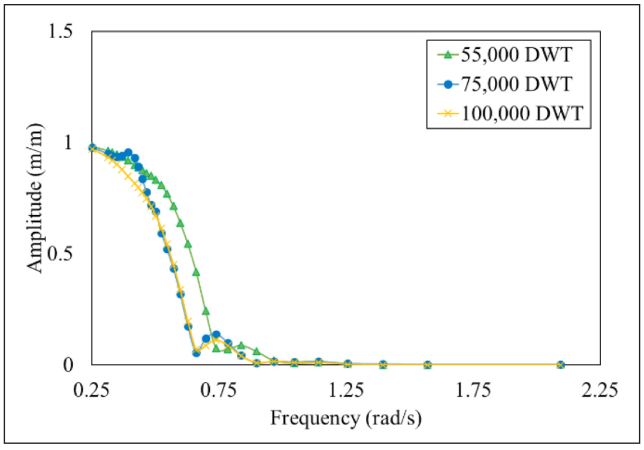

(e)

Figure 6 Comparison of heave RAO motions, a) stern seas (0°), b) following sea (180°), c) beam sea (90°), d) quartering seas (45°), and e) quartering sea (135°)

Table 8 Comparison of maximum RAO amplitude under different wave headings

Motions	DWT	Wave heading								Units
		Head sea / following seas		Beam seas		Quartering seas				
		0°	180°	90°	270°	45°	135°	225°	315°	
Surge	55.000	0.913	0.933	0.037	0.037	0.659	0.669	0.669	0.659	m/m
	75.000	0.893	0.917	0.035	0.035	0.655	0.664	0.664	0.655	
	100.000	0.882	0.907	0.035	0.035	0.649	0.661	0.657	0.652	
Sway	55.000	0	0	0.929	0.929	0.642	0.642	0.642	0.642	m/m
	75.000	0.004	0.004	0.926	0.926	0.632	0.631	0.631	0.632	
	100.000	0.005	0.005	0.944	0.945	0.643	0.646	0.647	0.644	
Heave	55.000	0.963	0.965	1.498	1.497	0.984	0.984	0.984	0.984	m/m
	75.000	0.943	0.946	1.471	1.47	0.976	0.978	0.978	0.977	
	100.000	0.935	0.938	1.419	1.418	0.969	0.971	0.97	0.972	
Roll	55.000	0	0	0.846	0.846	0.47	0.485	0.485	0.471	deg/m
	75.000	0.013	0.013	0.656	0.656	0.475	0.534	0.538	0.474	
	100.000	0.015	0.016	0.774	0.679	0.586	0.538	0.548	0.572	
Pitch	55.000	1.761	1.555	0.156	0.156	1.722	1.501	1.5	1.723	deg/m
	75.000	1.861	1.68	0.079	0.079	1.667	1.524	1.519	1.665	
	100.000	1.201	1.087	0.112	0.112	1.225	1.092	1.089	1.224	
Yaw	55.000	0	0	0.013	0.013	0.396	0.402	0.402	0.395	deg/m
	75.000	0.003	0.003	0.008	0.011	0.245	0.245	0.247	0.243	
	100.000	0.005	0.006	0.012	0.012	0.299	0.304	0.305	0.3	

wave-induced heave due to its smaller mass. However, the heave RAO patterns are generally consistent across different wave headings, suggesting that the vertical motion response of these Tankers is unaffected mainly by wave direction. This analysis highlights how vessel size and frequency impact the heave RAO, with larger vessels demonstrating enhanced stability against heave motion.

Table 8 reveals distinct patterns across motions, Tanker sizes, and wave headings. Surge, heave, and pitch motions show the most pronounced RAO values, with peak responses occurring in the head, following, and beam seas. Smaller vessels, such as the 55,000 DWT Tanker, are more susceptible to pitch and heave motions, while larger vessels, especially the 100,000 DWT Tanker, exhibit greater roll and yaw responses. The results suggest that vessel size plays a crucial role in moderating pitch and heave responses, with larger vessels generally exhibiting enhanced stability against vertical and longitudinal wave forces. This result highlights the impact of wave direction on Tanker stability, with heave and pitch being particularly sensitive to specific headings.

Figure 7 presents the RAO response for an SPM CALM buoy, illustrating the RAO responses for heave, surge, and pitch motions across a frequency range from 0.25 to 2.25 rad/s. The heave RAO, shown in Figure 7a, indicates a gradually decreasing trend in response amplitude as frequency increases. At lower frequencies, the heave response amplitude starts near 1 m/m, which suggests a resonant-like behavior where the buoy follows the wave amplitude closely. As the frequency approaches 2 rad/s, the amplitude falls to about 0.4 m/m, showing that the heave motion becomes less responsive to higher-frequency waves. This decline in amplitude at higher frequencies may be due to the buoy's natural heave resonance frequency lying below the tested range, leading to decreased heave efficiency as wave frequency increases.

In Figure 7b, the surge RAO exhibits a similar trend, with a peak amplitude close to 1 m/m at lower frequencies, which gradually reduces as the frequency increases. The surge amplitude drops significantly below 1 m/m by the upper end of the frequency range. This trend suggests that the buoy experiences strong surge motion at lower frequencies, likely due to the horizontal wave forces aligning with the natural surge characteristics of the CALM buoy system. However, as wave frequency increases, the surge response diminishes, which may reflect the system's reduced capacity to respond to higher-frequency forces.

Pitch RAO, depicted in Figure 7c, reveals a different pattern than heave and surge. Starting from a low amplitude at 0.25 rad/s, the pitch amplitude rises steadily

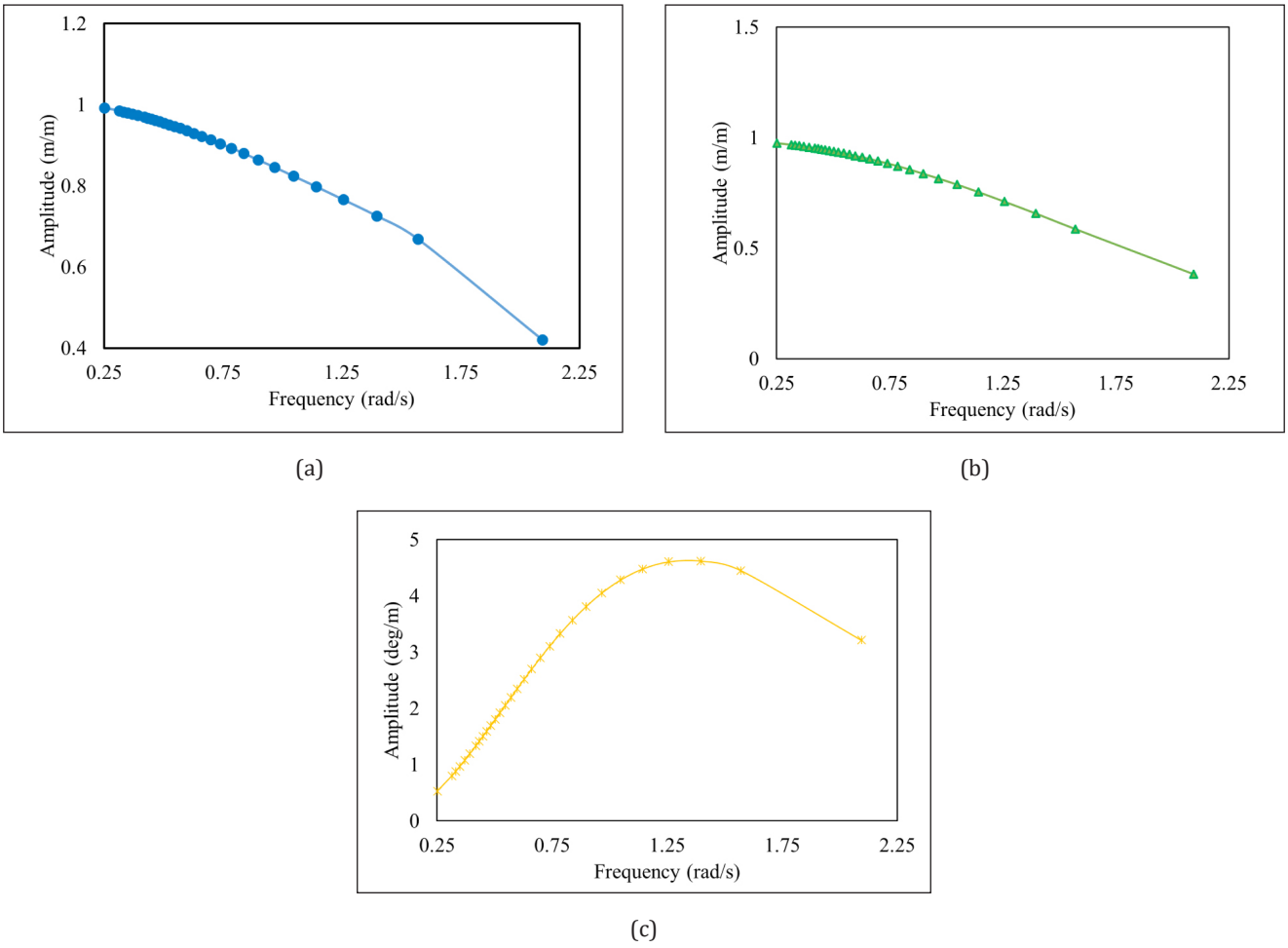

Figure 7 Comparison of RAO response of SPM CALM buoy, a) heave, b) surge, and c) pitch motions

and reaches a peak response amplitude of approximately 4.5 deg/m around 1.25 rad/s. After reaching this peak, the amplitude gradually decreases with further increases in frequency. This pattern indicates that the pitch motion is most responsive around the mid-frequency range, likely due to resonance effects associated with the buoy's rotational characteristics. The pronounced peak at 1.25 rad/s suggests that this frequency aligns closely with the natural pitch resonance of the buoy, causing the buoy to experience amplified rotational responses to wave forces at this frequency. Beyond this peak, the decline in amplitude indicates that the buoy is less responsive to pitch motions at higher frequencies.

3.3 Tension Analysis of SPM in Various Loading Conditions

In the tension analysis, this study investigates the maximum stress experienced by the six mooring lines of the SPM system, focusing particularly on the Y-connection plates on mooring lines 1 and 3. The mooring connections were analyzed assuming that the mooring system would be subjected to loads exceeding the SPM's capacity, simulating conditions where the connected vessel is larger than the SPM's designed operational capacity.

To achieve accurate stress and dynamic response predictions, the analysis employs a combination of fully integrated 3D diffraction theory and FEA. The 3D diffraction theory accounts for wave interaction with the floating structure. At the same time, the FEA framework is used to model the structural response of the mooring lines and components under applied loads. Time-domain dynamic analysis enables the simulation of transient responses, capturing the mooring system's behavior under variable wave and environmental conditions over time.

The three ship and SPM models are created at full scale and have been validated, as shown in Table 7. The simulation was conducted with a tension distribution for 10,800 seconds, following the guidelines in API RP 2SK and DNV OS E301 [35], [38]. The output includes time history data for eight wind loading directions relative to the compass, which are: stern (0°), quartering stern (45°), beam seas (90°), bow quartering (135°), head seas (180°), quartering seas (225°), beam seas (270°), and quartering seas (315°), as illustrated in Figure 9.

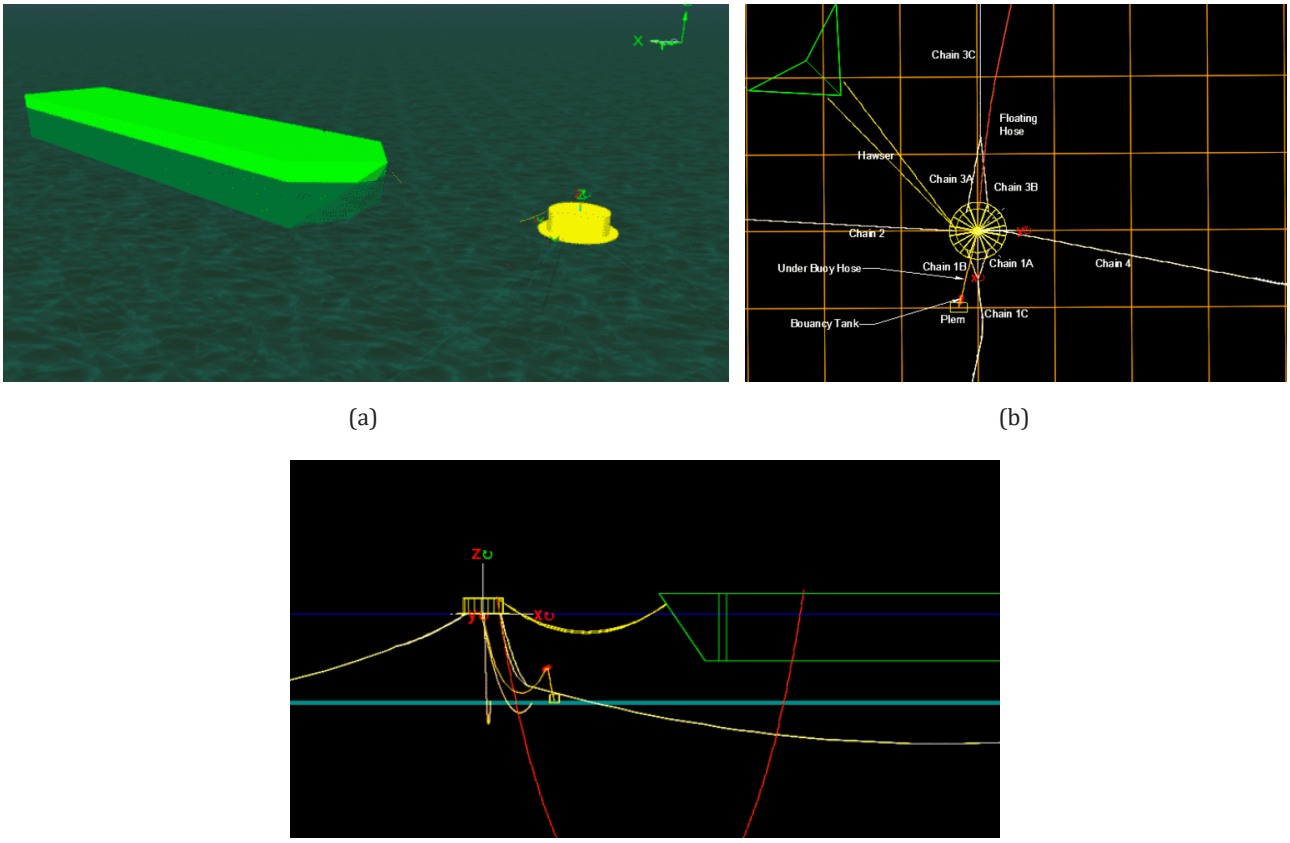

(a) (b)

(c)

Figure 8 Mooring conditions between SPM and Tanker, a) 3D view, b) top view, and (c) side view

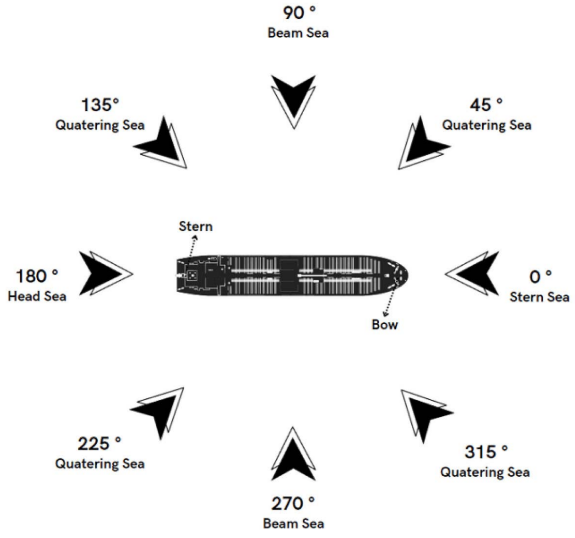

Figure 9 Tanker loading direction under different operating directions

All four condition variables were simulated, such as survival and moored conditions under different loads. The results indicate the tension in each mooring line for each vessel, with the analysis adhering to the API RP 2SK 4th Edition standard, which specifies a minimum safety factor of 1.67 for Ultimate Limit State (ULS) conditions. The mooring lines are analyzed across eight loading directions, with environmental data incorporated to ensure that results reach the desired accuracy level. The safety factor is calculated using an established formula supported by the minimum breaking load data for each mooring component.

Based on Figure 10, the safety factor calculation compares each mooring line's minimum breaking load standard with its maximum tension. According to API RP 2SK regulations, the safety factor must be at least 1.67. In this study, the maximum tension generated by the SPM CALM Buoy at Arubay, before Tanker mooring (survival condition), with a 100-year environmental load, is 38.43 tons on chain 2, at a heading of 270° (beam sea). Similar phenomenon can be found that the dynamic behavior of the mooring system is affected by the tanker's loading condition. Numerical simulations indicate that variations in tanker load can lead to significant changes in mooring line tension [40], [41]. Heavier loads can lead to higher tensions, which need to be managed to prevent line failure, ecessitating careful monitoring and adjustment of the mooring system to ensure operational safety [42], [43].

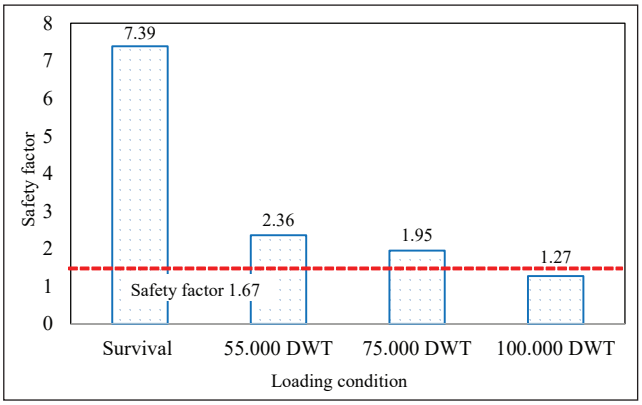

Figure 10 Mooring line safety factor for each loading scenario

In operating conditions, a 10-year environmental load is applied to evaluate the SPM's ability to endure loads beyond its rated capacity. For the first scenario, where the SPM CALM Buoy is moored to a 55,000 DWT Tanker, the maximum tension on chain 2 reaches 120.18 tons at a heading of 270° (beam sea). The resulting safety factor is 2.36, which meets the regulatory requirements for safe operation. In the second scenario, with the SPM CALM Buoy moored to a 75,000 DWT Tanker, the maximum tension reaches 145.47 tons on chain 4, at a heading of 90° (beam sea). This yields a safety factor 1.95, indicating safe operation under these conditions. For the final scenario, with the SPM moored to a 100,000 DWT Tanker, the maximum tension on chain 4 reaches 223.41 tons when the vessel is positioned at a 0° heading (stern sea). The resulting safety factor is 1.27, which falls below the safety threshold, indicating an unsafe operating condition for this load.

Figure 11 shows the time history of maximum tension in a mooring line for different loading conditions, including a survival scenario and operational scenarios with Tankers of varying deadweight tonnage. In the survival condition, represented by the red line, the tension remains consistently low and stable, with values staying below 500 kN throughout the 500 s period. This stability suggests minimal stress on the mooring line when the SPM is not actively moored to a Tanker, indicating that the system handles environmental loads well under these conditions.

In contrast, when the SPM is moored to a 55,000 DWT Tanker, tension increases noticeably, peaking slightly above 1,000 kN. The tension profile shows some fluctuation, particularly after around 75 seconds, but generally remains lower than in the scenarios with larger Tankers. These results imply that the mooring line can comfortably accommodate this load, with tension levels within an acceptable range.

The 75,000 DWT Tanker introduces even greater tension, reaching peaks around 1,500 kN. The tension fluctuates significantly, especially in the early part of the simulation (from around 100 to 200 seconds), indicating that the mooring system experiences more dynamic loading as the Tanker size increases. This higher and more variable tension suggests a greater demand on the mooring line, though it remains within a manageable range for this Tanker size.

The mooring line experiences the highest tension levels with the 100,000 DWT Tanker, with peaks approaching or exceeding 2,000 kN. Two significant peaks, around 100 and 300 seconds, indicate that the system endures substantial stress when handling a Tanker of this size. The fluctuations are more pronounced, reflecting the increased dynamic load and the proximity to the mooring line's load capacity. This aligns with the study's findings that the safety factor may fall below acceptable thresholds for the 100,000 DWT condition, posing an operational risk.

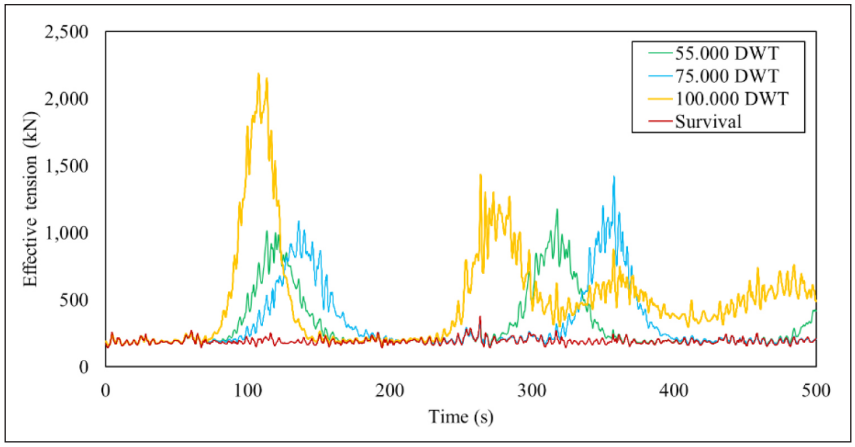

Figure 11 Time history of a maximum tension mooring line in stern sea load direction.

3.4 Strength Analysis on Y-connection in Various Loading Conditions

The tension analysis of the Y-connection was conducted using FEA software to analyze the stress contour of the model on different loading conditions. FEA using static linear analysis is used in this study. The Y-connection using steel high strength low alloy material was loaded to reflect operating conditions that impact the structure during operation. Figure 12 illustrates the boundary and loading conditions of the Y-connection, where holes A, B, and C are subjected to forces applied by shackles at specific angles. The boundary conditions for the Y-connection involve constraints imposed at certain points to control the system's response to the applied load. Fixed constraints were applied to the top and bottom surfaces of the Y-connection, as seen in Figure 12a. Forces were applied in three directions perpendicular to the each hole based on the force output from Orcaflex, as shown in Figure 12b. Load magnitudes of each load scenario is presented in Table 9 and material properties is presented in Table 10.

In the initial study, a mesh convergence analysis was conducted to determine the optimum mesh size by comparing the von Mises stress of the Y-connection under survival conditions. A mesh size range of 0.2 mm to 0.01 mm using 3D solid elements with triangular elements was evaluated. It was found that a mesh size of 0.01 mm, with a total of 280,787 elements and 402,682 nodes, was the most suitable.

Figure 12 presents the Von Mises stress contours on the Y-connection under various loading conditions, showing each scenario's stress distribution and maximum stress values. The images reveal how the Y-connection responds structurally to different Tanker sizes, highlighting areas of high-stress concentration, particularly around the connection holes labeled A, B, and C. In the survival condition in Figure 12a, the Y-connection experiences relatively low stress, with a maximum of 115.3 MPa. This scenario represents the baseline, where the Y-connection is subjected to minimal external loads, showing that the structure remains within safe limits. The highest stress is localized around holes B and C. However, the intensity is low, indicating that these points are more sensitive to load concentration but not

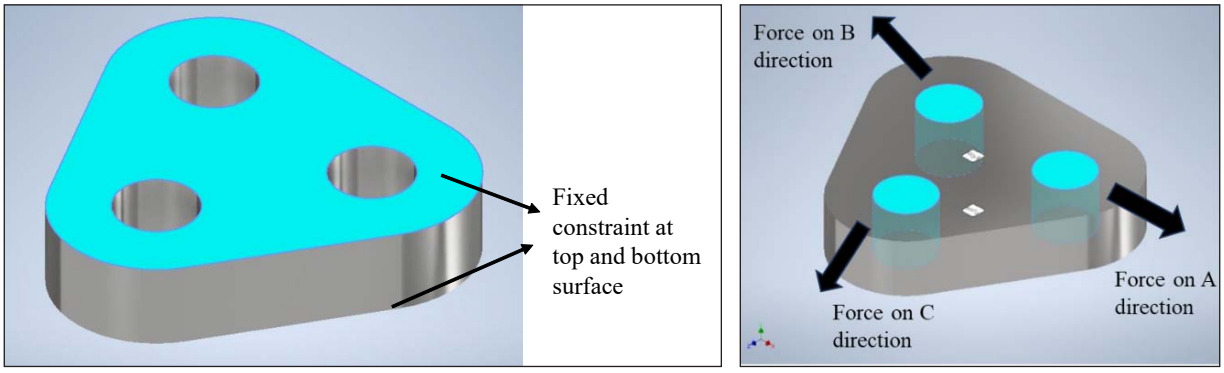

(a) (b)

Figure 12 a) Fixed boundary condition, b) operation condition on the Y-connection

Table 9 Load applied on Y-connection at operating condition on different load scenario

Load scenario	Force on A direction (N)	Force on B direction (N)	Force on C direction (N)
Survival	152.069	678.223	646.926
55,000 DWT Tanker	474.915	7042.793	1163
75,000 DWT Tanker	5224.509	77144.78	12795
100,000 DWT Tanker	91165.6	1282230.37	21746

Table 10 Material properties of Y-connection

Material	Steel High Strength Low Alloy (HSLA)
Young's Modulus (GPa)	200
Poisson's Ratio	0.287
Shear Modulus (GPa)	77.7001
Yield Strength (MPa)	275.8
Ultimate Strength (MPa)	448
Density (g/cm^3)	7.85
Area (m^2)	0.423
Volume (m^3)	0.010124

under significant strain in survival conditions. When moored to a 55,000 DWT Tanker in Figure 12b, the Y-connection's stress increases notably, with the maximum stress reaching 197.4 MPa. The stress concentration remains centered around holes B and C, showing that these areas endure more load as the Tanker size increases. Although the stress levels are higher, they indicate that the Y-connection operates safely under this load. For the 75,000 DWT Tanker scenario in Figure 12c, the Y-connection experiences even greater stress, with a maximum of 217.2 MPa. The contour around holes B and C appears denser, indicating that these areas are experiencing higher load concentrations. The increasing stress level reflects the additional strain on the structure, suggesting that the Y-connection is nearing a more demanding operational limit with this Tanker size. The highest stress level in the 100,000 DWT Tanker condition, as seen in Figure 12d, where the maximum stress on the Y-connection reaches 296.2 MPa. The stress distribution around holes B and C becomes significantly intense, showing dense and highly concentrated stress contours. This indicates that the Y-connection is under substantial load and approaching its structural capacity, with the potential for material fatigue or failure if exposed to further loads. The high-stress areas in this scenario suggest that the Y-connection may be at risk if operated continuously under such heavy loading conditions.

Figure 14 compares the Y-connection's structural response under varying loading conditions. The Von Mises stress and displacement increase as Tanker size and load conditions rise, with the stress reaching 369.2 MPa and displacement reaching 0.025 mm under the highest load condition. This upward trend suggests that the Y-connection experiences more significant stress and deformation as the load intensifies. This indicates a potential need for structural reinforcement when handling larger Tankers to prevent fatigue or failure.

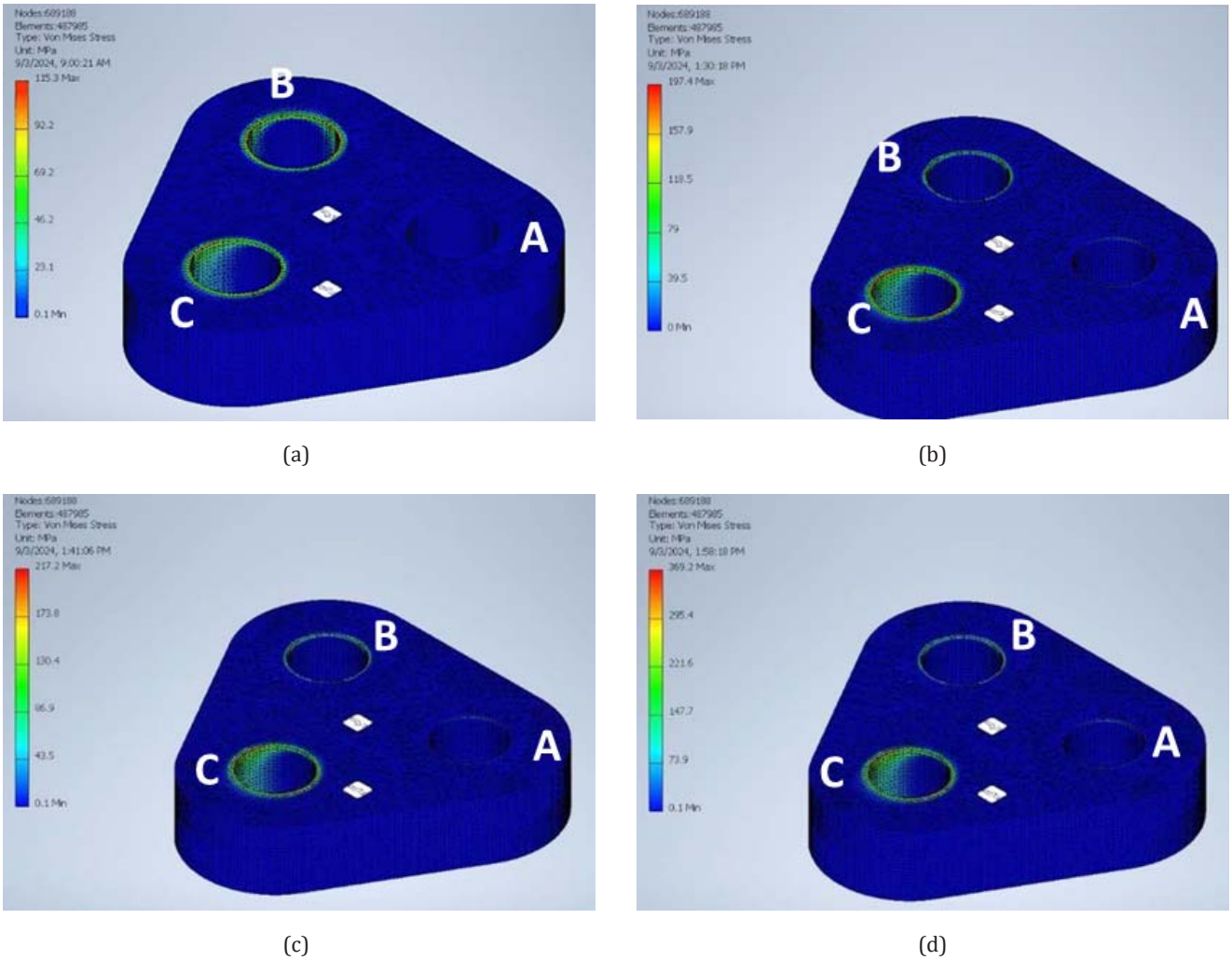

Figure 13 Von Mises stress contour at the Y-connection at different loading conditions, a) survival c, b) 55,000 DWT, c) 75,000 DWT, and d) 100,000 DWT

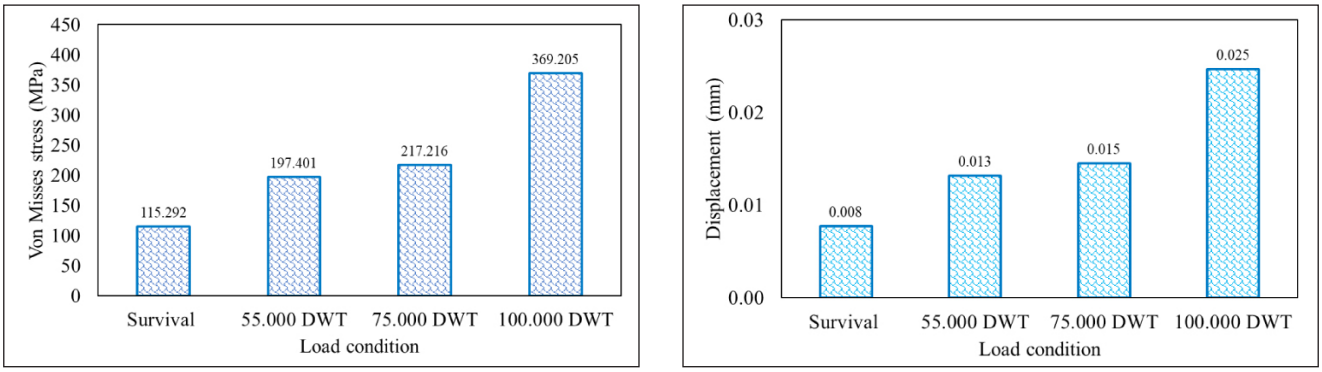

(a) (b)

Figure 14 Comparison of strength analysis on Y-connection at different loading conditions, a) von Mises stress, (b) displacement.

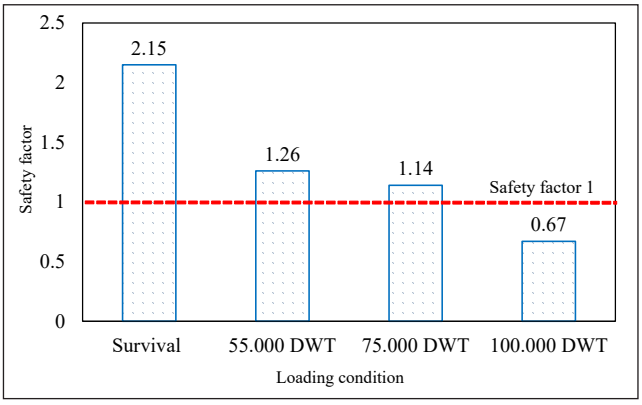

Figure 15 Safety factor on the Y-connection for each loading scenario

The safety factor for the Y-connection is calculated as yield strength of material in Table 10 to the maximum Von Mises stress. The analysis shows that survival and operational conditions for 55,000 DWT and 75,000 DWT ships fall within the safe category, as their safety factor values exceed 1, meeting the criteria set by ABS standard. However, for operational conditions with a 100,000 DWT ship, the Y-connection's safety factor falls below a safe threshold, indicating that it is not advisable to moor ships above 75,000 DWT on the SPM Arubay. The safety factor decreases significantly as the load increases beyond the SPM's capacity, highlighting a trend where increased moored loads reduce safety. Therefore, it is essential to benchmark the safety factor values against international standards, such as API RP 2SK, DNV OS E301, ABS standard, to ensure compliance and structural integrity.

4 Conclusion

The study provides insights into the hydrodynamic and structural responses of Tankers of varying deadweight tonnage when moored to an SPM CALM buoy. Heave and pitch RAO analysis revealed that smaller Tankers, such as the 55,000 DWT vessel, exhibit higher pitch and heave responses across a range of wave frequencies and headings. This increased sensitivity is attributed to the lower mass and moment of inertia, which heighten their response to wave-induced motions. Conversely, the 100,000 DWT Tanker shows significantly lower pitch and heave responses, demonstrating enhanced stability due to its larger mass and inertia. Wave direction also impacts motion, with head and following seas inducing notable pitch responses in smaller vessels, while larger vessels remain comparatively stable across most headings.

The tension analysis of the SPM's mooring lines under different loading conditions shows that safety factors vary significantly depending on the Tanker size and environmental load. For instance, under operational conditions with a 100,000 DWT Tanker, the safety factor for chain tension falls below the required threshold, signaling an unsafe condition. In contrast, the 55,000 DWT and 75,000 DWT conditions remain within safe operational limits, meeting the required standards for tension loads in survival and operational scenarios. Structural analysis of the Y-connection highlights stress concentrations around connection points, with larger Tanker sizes inducing higher stress levels. The 100,000 DWT Tanker scenario presents the highest stress, nearing the material's yield capacity, suggesting a risk of fatigue or failure under continuous high loads. The results underscore the critical role of vessel size, wave frequency, and heading on hydrodynamic responses and mooring line integrity. Larger Tankers contribute to reduced pitch and heave responses, enhancing stability, yet demand increased structural capacity from the mooring system. The findings advocate for caution when mooring vessels over 75,000 DWT to the SPM Arubay, as safety margins decrease with vessel size. Ensuring structural integrity for high loads requires adherence to international standards like API RP 2SK, DNV OS E301, and ABS to

maintain safe operational conditions and prevent structural fatigue in the SPM system.

Funding: This work was supported by the Institute for Research and Community Services (LPPM) Universitas Diponegoro, under the Research Scheme of World Class Research Universitas Diponegoro (WCRU), with research grant/contract no. 357-38/UN7.D2/PP/IV/2024. The authors gratefully acknowledge the support.

Conceptualization: Tuswan Tuswan; resources, Zulfaidah Ariany; data collection, Adam Adam, Alfiy Alfatarizqi; writing-original draft preparation, Berlian Arswendo Adietya; writing-review and editing, Tuswan Tuswan; supervision, Ahmad Fauzan Zakki, Aulia Windyandari. All authors have read and agreed to the published version of the manuscript.

Competing Interests: The authors declare no competing interest.

References

[1] L. Sun, X. Zhang, Y. Kang, and S. Chai, "Motion Response Analysis of FPSO's CALM Buoy Offloading System," in *n International Conference on Offshore Mechanics and Arctic Engineering (Vol. 56598, p. V011T12A008)*, American Society of Mechanical Engineers., May 2015. doi: https://doi.org/10.1115/OMAE2015-41725.

[2] A. M. Cruz and E. Krausmann, "Damage to offshore oil and gas facilities following hurricanes Katrina and Rita: An overview," *J Loss Prev Process Ind*, vol. 21, no. 6, pp. 620–626, Nov. 2008, doi: https://doi.org/10.1016/j.jlp.2008.04.008.

[3] J. F. Wilson, "Offshore Structures (Marine Engineering)," *Encyclopedia of Physical Science and Technology*, pp. 161–168, 2003, doi: 10.1016/B0-12-227410-5/00512-3.

[4] L. Zhang, X. Zhen, Q. Duan, Y. Huang, C. Chen, and Y. Li, "Hydrodynamic Characteristics Analysis and Mooring System Optimization of an Innovative Deep-Sea Aquaculture Platform," *Journal of Marine Science and Engineering 2024, Vol. 12, Page 972*, vol. 12, no. 6, p. 972, Jun. 2024, doi: 10.3390/JMSE12060972.

[5] Z. Zhang, M. H. Kim, and E. G. Ward, "Progressive mooring-line failure of a deepwater MODU in hurricane conditions," in *ASME 2009 28th International Conference on Ocean, Offshore and Arctic Engineering*, Hawaii, USA: American Society of Mechanical Engineers, 2009. doi: https://doi.org/10.1115/OMAE2009-79794.

[6] M. H. Kim and Z. Zhang, "Transient effects of tendon disconnection on the survivability of a TLP in moderate-strength hurricane conditions," *International Journal of Naval Architecture and Ocean Engineering*, vol. 1, no. 1, pp. 13–19, Sep. 2009, doi: https://doi.org/10.2478/ijnaoe-2013-0002.

[7] C. K. Yang and M. H. Kim, "Transient effects of tendon disconnection of a TLP by hull-tendon-riser coupled dynamic analysis," *Ocean Engineering*, vol. 37, no. 8–9, pp. 667–677, Jun. 2010, doi: https://doi.org/10.1016/j.oceaneng.2010.01.005.

[8] A. Elhanafi, G. Macfarlane, A. Fleming, and Z. Leong, "Intact and Damaged Survivability of an Offshore Floating–moored OWC Device," in *27th (2017) annual International Offshore and Polar Engineering Conference*, San Francisco: International Society of Offshore and Polar Engineers, Jun. 2017, pp. 58–65.

[9] E. Malayjerdi, A. Ahmadi, and M. R. Tabeshpour, "Dynamic Analysis of TLP in intact and damaged tendon conditions," in *The 18th Marine Industries Conference (MIC2016)*, Kish Island, Oct. 2016, pp. 18–21. [Online]. Available: https://www.researchgate.net/publication/308794664.

[10] J. Yu, S. Hao, Y. Yu, B. Chen, S. Cheng, and J. Wu, "Mooring analysis for a whole TLP with TTRs under tendon one-time failure and progressive failure," *Ocean Engineering*, vol. 182, pp. 360–385, Jun. 2019, doi: https://doi.org/10.1016/j.oceaneng.2019.04.049.

[11] D. Qiao, B. Li, J. Yan, Y. Qin, H. Liang, and D. Ning, "Transient responses evaluation of FPSO with different failure scenarios of mooring lines," *J Mar Sci Eng*, vol. 9, no. 2, pp. 1–34, Jan. 2021, doi: https://doi.org/10.3390/jmse9020103.

[12] Murdjito, M. P. Rosari, and E. B. Djatmiko, "Analysis on the Critical Conditions of Side-by-Side Offloading Operation between SSP Type-FPSO and Shuttle Tanker," *Applied Mechanics and Materials*, vol. 874, pp. 53–63, Jan. 2018, doi: https://doi.org/10.4028/www.scientific.net/AMM.874.53.

[13] T. Bunnik, G. De Boer, J. Cozijn, J. Van Der Cammen, E. van Haaften, and E. ter Brake, "Coupled Mooring Analysis and Large Scale Model Tests on a Deepwater Calm Buoy in Mild Wave Conditions," in *21st International Conference on Offshore Mechanics and Arctic Engineering, Volume 1*, Oslo, Norway: American Society of Mechanical Engineers, Jun. 2022, pp. 65–6. doi: https://doi.org/10.1115/OMAE2002-28056.

[14] E. A. Tannuri, F. G. S. Torres, H. Igreja, and I. Q. Masetti, "FPSO and monobuoy offloading operation with a conventional shuttle tanker: Dimensioning of tugboat based on numerical simulation," in *IFAC Proceedings Volumes*, IFAC Secretariat, 2009, pp. 134–139. doi: https://doi.org/10.3182/20090916-3-BR-3001.0031.

[15] G. Rutkowski, "A comparison between conventional buoy mooring CBM, single point mooring SPM and single anchor loading sal systems considering the hydro-meteorological condition limits for safe ship's operation offshore," *TransNav*, vol. 13, no. 1, pp. 187–195, Mar. 2019, doi: 10.12716/1001.13.01.19.

[16] Y.-L. Hwang, "Dynamic Analysis for the Design of CALM System in Shallow and Deep Waters," *ASME. J. Offshore Mech. Arct. Eng*, vol. 3, no. 119, pp. 151–157, Aug. 1997, doi: https://doi.org/10.1115/1.2829062.

[17] C. V. Amaechi, C. Chesterton, H. O. Butler, F. Wang, and J. Ye, "Review on the design and mechanics of bonded marine hoses for Catenary Anchor Leg Mooring (CALM) buoys," *Ocean Engineering*, vol. 242, p. 110062, Dec. 2021, doi: 10.1016/J.OCEANENG.2021.110062.

[18] X. Ju, C. V. Amaechi, B. Dong, X. Meng, and J. Li, "Numerical analysis of fishtailing motion, buoy kissing and pullback force in a catenary anchor leg mooring (CALM) moored tanker system," *Ocean Engineering*, vol. 278, p. 114236, Jun. 2023, doi: 10.1016/J.OCEANENG.2023.114236.

[19] J. Fan, H. Bai, M. Wang, and H. Fang, "Research on cable dynamic response of a catenary anchor leg mooring system based on ANCF," *Ocean Engineering*, vol. 305, Aug. 2024, doi: 10.1016/j.oceaneng.2024.117916.

[20] J. Fan, H. Bai, M. Wang, and H. Fang, "Research on cable dynamic response of a catenary anchor leg mooring system based on ANCF," *Ocean Engineering*, vol. 305, Aug. 2024, doi: https://doi.org/10.1016/j.oceaneng.2024.117916.

[21] Q. Sun *et al.*, "Anchor Chain Optimization Design of a Catenary Anchor Leg Mooring System Based on Adaptive Sampling," *J Mar Sci Eng*, vol. 10, no. 11, Nov. 2022, doi: https://doi.org/10.3390/jmse10111739.

[22] L. V. S. Sagrilo, M. Q. Siqueira, G. B. Ellwanger, E. C. P. Lima, A. S. Ferreira, and M. M. Mourelle, "A coupled approach for dynamic analysis of CALM systems," *Applied Ocean Research*, vol. 24, no. `1, pp. 47–58, Feb. 2002, doi: https://doi.org/10.1016/S0141-1187(02)00008-1.

[23] H. Huang and H. C. Chen, "Coupled CFD-FEM simulation for the wave-induced motion of a CALM buoy with waves modeled by a level-set approach," *Applied Ocean Research*, vol. 110, p. 102584, May 2021, doi: 10.1016/J.APOR.2021.102584.

[24] "Standards Manager Web Standards List SHELL-Shell Oil Company."

[25] C. V. Amaechi, F. Wang, and J. Ye, "Mathematical modelling of bonded marine hoses for single point mooring (Spm) systems, with catenary anchor leg mooring (calm) buoy application—a review," *J Mar Sci Eng*, vol. 9, no. 11, Nov. 2021, doi: https://doi.org/10.3390/jmse9111179.

[26] J. F. Flory and P. F. Poranski, "The Design of Single Point Moorings," in *OTC-2827-MS*, Offshore Technology Conference, May 1977. doi: https://doi.org/10.4043/2827-MS.

[27] Y. Zhao, L. S. Hao, and L. Wan, "Research on the spatial structure of crude oil flow and the characteristics of its flow field in China," *Energy Policy*, vol. 35, no. 10, pp. 5035–5050, Oct. 2007, doi: https://doi.org/10.1016/j.enpol.2007.03.022.

[28] J. G. Speight, "Offshore Platforms," *Subsea and Deepwater Oil and Gas Science and Technology*, pp. 71–106, Jan. 2015, doi: 10.1016/B978-1-85617-558-6.00003-9.

[29] C. J. Ehlers, A. G. Young, and J. Chen, "Technology Assessment of Deepwater Anchors," in *Offshore Technology Conference*, Houston, Texas, May 2004. doi: https://doi.org/10.4043/16840-MS.

[30] X. Qi, Chen Yongkun, Q. Yuan, G. Xu, and K. Huang, "Calm Buoy and Fluid Transfer System Study," in *Proceedings of the Twenty-seventh (2017) International Ocean and Polar Engineering Conference*, San Francisco, CA, USA: International Society of Offshore and Polar Engineers, Jun. 2017. Accessed: Apr. 09, 2025. [Online]. Available: https://onepetro.org/ISOPEIOPEC/proceedings-abstract/ISOPE17/All-ISOPE17/ISOPE-I-17-128/17225?redirectedFrom=PDF

[31] I. J. L. Cozijn and I. T. H. J. Bunnik, "Coupled Mooring Analysis for a Deep Water CALM Buoy," *Proceedings of the International Conference on Offshore Mechanics and Arctic Engineering - OMAE*, vol. 1 B, pp. 663–673, Dec. 2008, doi: 10.1115/OMAE2004-51370.

[32] T. Dewhurst, S. Hallowell, and C. Newell, "Dynamics of an Array of Submersible Mussel Rafts in Waves and Current," in *Proceedings of the ASME 2019 38th International Conference on Ocean, Offshore and Arctic Engineering*, Glasgow, Scotland: American Society of Mechanical Engineers, Jun. 2019. doi: https://doi.org/10.1115/OMAE2019-96388.

[33] Y. Haditiar, M. Ikhwan, M. Nanda, and H. A. Haridhi, "Understanding sea wave height conditions in sumatra waters," in *BIO Web of Conferences*, EDP Sciences, Jan. 2024. doi: 10.1051/bioconf/20248702014.

[34] H. Bandringa, F. Jaouën, J. Helder, and T. Bunnik, "On the Validity of CFD for Simulating a Shallow Water CALM Buoy in Extreme Waves," *Proceedings of the International Conference on Offshore Mechanics and Arctic Engineering - OMAE*, vol. 1, Oct. 2021, doi: 10.1115/OMAE2021-62738.

[35] API Recommended Practice 2SK, "Design and Analysis of Stationkeeping Systems for Floating Structures, Third Edition," Washington D.C, 2008.

[36] M. L. Simão, L. V. S. Sagrilo, P. M. Videiro, and M. C. de Oliveira, "An ULS reliability-based design method for mooring lines using an efficient full long-term approach," *Marine Structures*, vol. 99, p. 103718, Jan. 2025, doi: 10.1016/J.MARSTRUC.2024.103718.

[37] I. P. S. Asmara, Sumardiono, and V. A. P. Wibowo, "Safety Analysis of Mooring Hawser of FSO and SPM Buoy in Irregular Waves," *IOP Conf Ser Earth Environ Sci*, vol. 557, no. 1, p. 012003, Aug. 2020, doi: 10.1088/1755-1315/557/1/012003.

[38] DNV GL, "DNVGL-OS-E301 Position mooring," Jul. 2015. [Online]. Available: www.dnvgl.com.

[39] American Bureau of Shipping, "ABS Rules for Building and Classing Mobile Offshore Drilling Units and The 1989 IMO MODU Code," Nov. 1998. Accessed: Mar. 19, 2025. [Online]. Available: https://www.dco.uscg.mil/Portals/9/DCO%20Documents/5p/5ps/Alternate%20Compliance%20Program/absmodu.pdf

[40] R. A. Khodr, R. S. Shiban, B. A. Nawaz, S. P. Mistry, and S. Aramco, "Reliability of Very Large Crude Carrier and Single Anchor Leg Mooring BuoyMooring System during Squall Event," in *Proceedings of the Annual Offshore Technology Conference*, 2020.

[41] R.-Y. Yang and W.-C. Chiang, "Dynamic motion response of an oil tanker moored with a single buoy under different mooring system failure scenarios," *Ships and Offshore Structures*, vol. 18, no. 7, pp. 923–936, 2023, doi: 10.1080/17445302.2022.2082105.

[42] A. Gaffney and I. Bellamy, "Operational metocean monitoring at Catenary Anchor Leg Mooring (CALM) buoy," in *Proceedings of the International Offshore and Polar Engineering Conference*, 2004, pp. 157–162.

[43] H. Song, G.-A. Chang, T. Hou, and J. Zhang, "Dynamic analysis of calm buoy-based steel offloading line system," in *19th Offshore Symposium 2014: Emerging Technologies in Offshore Drilling and Production*, 2014, pp. 292–304.